

# Temperature and electric field dependence of spin relaxation in graphene on SrTiO<sub>3</sub>

Si Chen,\* Roald Ruiters, Vikramaditya Mathkar, Bart J. van Wees, and Tamalika Banerjee†  
*Zernike Institute for Advanced Materials,  
 University of Groningen, Nijenborgh 4,  
 9747 AG Groningen, The Netherlands*

(Dated: December 14, 2024)

The theoretically predicted intrinsic spin relaxation time of up to 1  $\mu$ s in graphene along with extremely high mobilities makes it a promising material in spintronics. In spite of extensive experimental studies of spin relaxation and understanding of its precise mechanism, it is still unclear as to why the spin lifetime in graphene is three orders of magnitude below the theoretical predictions. Central to this discrepancy is the role of the local environment including that of the underlying substrate. In this work, we use the electronically rich platform SrTiO<sub>3</sub> and study its suitability in supporting spin transport in graphene. We find spin relaxation time and length as large as  $1.2 \pm 0.1$  ns and  $5.6 \pm 0.5$   $\mu$ m respectively at 290 K in graphene on SrTiO<sub>3</sub> using a non-local measurement scheme. We analyze the temperature variation of the spin transport parameters in graphene and attribute the temperature dependence of the spin transport parameters in graphene to spin orbit coupling or structural phase transition in SrTiO<sub>3</sub>. Furthermore, from the gate dependence of the spin transport parameters, the relation between spin relaxation time and momentum relaxation time is extracted; the Elliot-Yaffet and D'Yakonov-Perel' spin relaxation rates are found to be of similar order.

**PACS numbers:**

Charge conduction and spin transport parameters in two-dimensional graphene are strongly influenced by extrinsic factors related to their local environment. Extrinsic influences range from adatoms,[1] the specifics of the underlying substrate (suspended, encapsulated or high dielectric constant), [1, 2] to the quality of the contacts.[3, 4] Specifically, the properties of the substrate can have their imprint on the electronic properties in graphene. For example, on an atomically flat two dimensional hexagonal Boron Nitride (hBN) substrate, an enhancement of the charge and spin transport parameters in graphene are observed.[5–8] Further, tunable spin-orbit interaction can be induced in graphene using WS<sub>2</sub> as a substrate.[9] Thus functionalizing graphene on different substrates is interesting for the design and development of multifunctional devices and for studying their (opto-)spin transport.

In this context SrTiO<sub>3</sub> (STO) is an interesting choice as a substrate.[10] STO has an atomically flat surface, similar to that of hBN, with roughness of 90 -150 pm and no dangling bonds. Moreover, unlike hBN, STO is electronically versatile. This stems from the remarkably large dielectric constant ( $\epsilon_r$ ) of 300 at room temperature that increases non-linearly to  $> 20,000$  at 4 K.[11] Further, distinct from most other substrates on which charge and spin transport in graphene has been studied, the broken inversion symmetry at the surface of STO leads to Rashba spin orbit fields that can be tuned by an electric field. [12] Recently it was demonstrated that electric dipoles, formed at the surface of STO, lead to a large out

of plane electric polarization that influences the charge transport in graphene. [13]

STO undergoes a ferroelastic transition changing from cubic ( $a = 3.905$  Å) to tetragonal symmetry ( $c/a = 1.0056$ ) at  $T = 105$  K.[14] This is accompanied by structural domains that can be moved with an external gate-bias.[15, 16] While the high  $\epsilon_r$  in STO can screen Coulomb potentials originating from impurities on the substrate or on graphene, the movement of structural ferroelastic domains in STO at low temperatures, can lead to potential modulations that causes local fluctuations in the carrier density of graphene. Thus STO offers an electronically rich transport platform for graphene-based devices. Recent studies on the charge transport in graphene on STO have been done [17–22] to understand the influence of the high  $\epsilon_r$  and its role in screening impurities and improving the charge mobility,  $\mu$ , in graphene.[23] However, the first experiments by Couto *et al.* did not show as large of an increase in mobility as graphene on SiO<sub>2</sub>. It was shown that the mobility of graphene is not limited by impurities of an electrostatic nature, which can be screened by STO, but rather by pseudomagnetic fields induced by random strain fluctuations from the substrate.[18] Furthermore, Sachs *et al.* studied the charge transport at 4 and 300 K and observed a slight increase in the mobility at low carrier densities and a hysteresis in the sheet resistance upon applying a gate voltage.[19] More recently, Kang *et al.* reported that gate induced oxygen vacancies in STO have important influence on the charge transport. [21]

Interestingly, in spite of the above studies, the influence of temperature and electric field driven structural and electronic phase transition in STO, as well as the large intrinsic Rashba spin orbit fields on spin transport

\* s.chen@rug.nl

† t.banerjee@rug.nl

in graphene is largely unknown. In this work, we study the spin transport in graphene on STO for the first time and investigate the effects of temperature and electric field using spin injection contacts of  $\text{Co}/\text{AlO}_x$ . We show that the spin relaxation time at 290 K is as long as  $1.2 \pm 0.1$  ns, with a spin relaxation length of  $5.6 \pm 0.5$   $\mu\text{m}$ . To investigate the role of the surface dipoles and the large, temperature dependent, non-linear dielectric constant on spin transport in graphene and across the ferroelastic transition in STO, spin transport measurements are performed at different temperatures. A nontrivial temperature dependence of spin parameters, characterized by spin lifetime and diffusion constant is observed. We observe the spin transport parameters to be lower at 4 K than at 290 K- an observation that has not been reported on other substrates such as SiC or  $\text{SiO}_2$ . Furthermore, we find that the gate dependence of the spin relaxation parameters at 4 K can be associated with the modulation of the strength of surface dipoles in STO. From an analysis of the spin relaxation mechanisms, we obtain a similar order of spin relaxation rates induced by the Elliot-Yaffet and D'Yakonov-Perel' mechanisms.

To investigate spin transport in graphene on STO, lateral spin valves of exfoliated graphene on  $\text{TiO}_2$  terminated STO were fabricated. One side polished STO (100) substrates (Crystec GmbH) were treated with a standard protocol [24, 25] to achieve a  $\text{TiO}_2$  terminated surface. An atomic force microscope (AFM) scan of one such terminated STO surface is shown in figure 1a. Graphite (grade ZYA) was exfoliated on a clean  $\text{SiO}_2/\text{Si}$  wafer and single layer graphene was selected based on optical contrast. These flakes were transferred from the  $\text{SiO}_2$  to the desired area on the STO substrate using a polycarbonate dry pick-up technique.[26] Polycarbonate residues left behind after the transfer were removed by treating the substrate at  $50^\circ\text{C}$  with chloroform for a period of several hours to days. Electrical contacts were defined using electron beam lithography and deposited using electron beam evaporation in multiple steps. A tunnel barrier was deposited in a two-step process: first 0.4 nm of aluminium was deposited and oxidized for 10 minutes in a pure oxygen atmosphere. This step was repeated once more to obtain a  $\sim 1$  nm thick  $\text{AlO}_x$  tunnel barrier. Thereafter 35 nm of ferromagnetic cobalt was deposited and capped with 5 nm aluminum layer to prevent cobalt from oxidizing. The substrate was bonded on a chip carrier using silver paste, which serves as the back gate during our transport measurements. An optical image of the device is shown in figure 1b.

Spin transport measurements were performed on the device, using a non-local geometry. This geometry, as shown in figure 1c, separates the charge current path from the voltage contacts to exclude spurious signals. The center to center separation between contacts 2 and 3 is 4.8  $\mu\text{m}$ . In this configuration both spin valve as well as Hanle precession measurements can be performed. Assuming  $\varepsilon_r$  in STO to be 24000, we calculate the mobil-

ity  $\mu$  of the sample to be  $658 \text{ cm}^2/\text{Vs}$  at 4 K obtained using  $\mu = 1/e d\sigma/dn$ . Spin valve measurements were performed by sweeping an in-plane magnetic field  $B$  in the  $y$ -direction and measuring the non-local resistance  $R_{\text{NL}} = V/I$ , using lock-in techniques with frequencies  $< 15$  Hz. [27] Figure 1d shows the response of one of the non-local spin valves at 290 K. Three switches are present which corresponds to contacts 1, 3, and 2, respectively.

Additionally Hanle precession measurements were performed, shown in figure 2a, for two magnetic configurations of the electrodes  $\downarrow\uparrow\uparrow$  and  $\uparrow\uparrow\uparrow$  for the contacts 1, 2, 3 ( $\uparrow, \downarrow$  refers to the magnetization of the electrodes in  $y$  and  $-y$  direction respectively), and the  $B$ -field is swept out-of-plane ( $z$ -direction), while measuring  $R_{\text{NL}}$ . Spins injected at contact 3 will start to precess around the  $B$ -field, thereby changing the projected spin component along the  $y$ -direction where they are detected by contacts 1-2. The resultant Hanle curves of  $\downarrow\uparrow\uparrow$  and  $\uparrow\uparrow\uparrow$  configurations are shown in figure 2b (black curve and red curve respectively). A common background is subtracted to obtain the pure spin signal using:  $R_s = 1/2(R_{\downarrow\uparrow\uparrow} - R_{\uparrow\uparrow\uparrow})$  as detailed in [5]. The blue curve in figure 2b shows the data after background subtraction. Thereafter, it was fitted with the steady state solution to the Bloch equation in the diffusive regime.[27, 28] From this, the spin diffusion constant  $D_s$  and the spin relaxation time  $\tau_s$  were obtained and the spin relaxation length was calculated using:  $\lambda_s = \sqrt{D_s \tau_s}$ . We find  $\tau_s = 1.2 \pm 0.1$  ns,  $D_s = 0.027 \pm 0.004 \text{ cm}^2/\text{s}$  and  $\lambda_s = 5.6 \pm 0.5$   $\mu\text{m}$ . These values are comparable to that of graphene on hBN substrate.[5] This demonstrates the efficacy of STO as a suitable platform to study spin transport in graphene on STO.

In order to investigate the influence of temperature driven electronic and structural phase transitions in STO on spin transport in graphene, we have performed temperature dependent Hanle measurements. Before starting the spin transport measurements, a back gate was swept between  $0 \text{ V} \sim -70 \text{ V} \sim 70 \text{ V} \sim 0 \text{ V}$  at 4 K in order to characterize the charge transport properties in graphene on STO (see supplementary information figure S2). Thereafter spin transport measurements were carried out while heating up the device. The measurements were performed using the non-local geometry (figure 2b) in a temperature range between 4 and 290 K. We see that the spin relaxation time,  $\tau_s$ , shows a maximum at around 180 K and decreases slightly beyond this. The variation of the spin diffusion constant,  $D_s$ , with temperature is different from that of the spin relaxation time as shown in figure 2b. The calculated value of the spin relaxation length,  $\lambda_s$ , shows a maximum value of 7  $\mu\text{m}$  at 180 K. We have observed a similar trend in the temperature dependence of spin transport, but with a shorter spin relaxation time, on other STO substrates.

The spin transport parameters are usually known to decrease with increasing temperature, due to a reduction in the electron-phonon scattering. Earlier studies[3, 4] report a decrease of spin transport parameters with increasing temperature on SiC and Si substrate respectively,

which is due to the enhanced electron-phonon scattering at higher temperature. However, we observe a different trend here : the spin relaxation time for temperatures above 180 K is almost twice as large as that in the temperature regime of 30-120 K. To understand this variation, we first look into the dependence of the carrier density and the changes in the square resistance of graphene with temperature. This is shown in figure 3 for the contacts studied in figure 2b. In the temperature regime (30-180 K) where the variation is the largest, we find that graphene is set in the metallic state at zero gate voltage. This is evident from the temperature dependence of charge transport. The carrier density  $n$  is calculated using Einstein relation  $\sigma = e^2\nu D_c$ , assuming  $D_c \sim D_s$ :

$$n = \frac{(\hbar v_F)^2 \pi}{g_s g_v D_s^2 R_{sq}^2 e^4} \quad (1)$$

where  $R_{sq}$  is the square resistance of graphene,  $v_F$  is the Fermi velocity,  $\hbar$  is the reduced Plank constant,  $g_s = 2$ ,  $g_v = 2$  are the spin and valley degeneracy respectively,  $D_c$  is the charge diffusion coefficient and  $\nu$  is the density of states at the Fermi energy. The calculated carrier density varies between  $3 \times 10^{12} \text{cm}^{-2}$  -  $1 \times 10^{13} \text{cm}^{-2}$  (figure 3b) in this temperature range and is consistent with other similarly fabricated devices in a Hall bar geometry ( $10^{12} \text{cm}^{-2}$  -  $10^{13} \text{cm}^{-2}$ ). The observed fluctuation of the carrier density with temperature is mainly attributed to the uncertainty in the determination of  $D_s$ . The determination of  $D_s$  is sensitive to the detailed structure of the Hanle curve and is much more sensitive than the determination of  $\tau_s$ . In equation 1,  $n$  varies as  $\frac{1}{D_s^2}$  and  $D_s$  is obtained from the fitting of the Hanle data. Any uncertainty in the determination of  $D_s$  is thus amplified in the calculation of  $n$ . Possible errors due to such fitting procedure are difficult to determine. Hence, given the uncertainty in the fitting procedure, a temperature independence of carrier density cannot be strictly excluded. Despite the large carrier density fluctuation, the important point is that the graphene is in a high carrier density regime, where the change in carrier density does not have a big influence on the spin relaxation in graphene.

To study the contribution of spin absorption to the observed variation of the spin lifetime, we next discuss the invasiveness of the contacts with temperature. The injected spins from the low resistive ferromagnetic electrode to the high resistive channel can be backscattered into the electrodes depending on the ratio between the resistance of the contact and spin transport channel. Thus a change in either the contact resistance ( $R_c$ ) or in the channel resistance ( $R_{sq}$ ), measured in a three probe measurement geometry, can lead to a change in the extracted spin transport parameters. In our case, we measure contact resistances of 8 k $\Omega$ , 21 k $\Omega$ , 22 k $\Omega$  and 13 k $\Omega$  for contacts 1, 2, 3, 4 respectively and find that both the contact resistance and square resistance have very little fluctuation with temperature. To further investigate this, the invasiveness of the contacts is evaluated using the R pa-

rameter,  $R = (R_c/R_{sq})W$ , where  $W$  is the width of the graphene channel.[4]  $R/\lambda_s$  varies from 1.1 to 3.5 (for  $L/\lambda_s = 0.9 \sim 1.6$ ) and as discussed in reference [4], such a fluctuation in  $R/\lambda_s$  can maximally contribute to a change of 20 % in the spin transport parameters, (shown in figure S3 in supplementary information). Thus it can be inferred that the invasiveness of the contacts does not play a crucial role in the observed temperature variation of the spin transport parameters.

A possible explanation for the reduction in spin relaxation times at low temperatures can be found when we take into account the role of spin-orbit coupling in STO. An electric field induced (via spin orbit coupling) change in the spin relaxation time has been demonstrated earlier in graphene and also in doped-STO.[2, 12] In our case, the origin of the electric field is intrinsic to the STO substrate. The surface of STO has a broken inversion symmetry and is found to harbor surface dipoles where the oxygen atoms are displaced outwards.[19, 29] The strength of these surface dipole moments is calculated to be  $P = -13.89 \mu\text{C}/\text{cm}^2$  which increases to  $P = -34.90 \mu\text{C}/\text{cm}^2$  with the graphene layer. [13, 30] The electric field originating from the surface dipoles can be enhanced by the increased  $\epsilon_r$  in STO at low temperatures. This transverse intrinsic electric field effectively influences the spin relaxation time in graphene via spin-orbit coupling. With increasing temperature, and a reduction of the surface electric field due to the slow relaxation of the surface dipoles [19], the spin relaxation time is found to increase. At temperatures above 200 K, the electron phonon scattering plays an important role, leading to a decrease of  $\tau_s$ ,  $D_s$ ,  $\lambda_s$ . Note that resonant scattering due to impurity scattering centers, as discussed by Kochan *et al.* [31], has a weaker influence on the spin relaxation time with temperature, unlike what we observe.

Additional factors such as the structural transition in STO at 105 K, leading to the formation of long striped domains and inducing rumpling on the graphene surface, are important to understand the temperature dependence of electronic transport in graphene on STO. Recent studies show that below the cubic to tetragonal phase transition temperature of 105 K, differently oriented large (micron size) tetragonal domains are formed in STO where the local electrostatics are different than at the domain walls. [15, 16] These will induce potential modulations across the graphene sheet (see the charge transport data in figure S2) and will vary strongly with temperature. These local rumplings will act as additional local scattering centers at low temperatures. The induced rumpling of the graphene surface will gradually relax with increasing temperature with an annihilation of the tetragonal domains at temperatures above 105 K, thus influencing spin transport in graphene.

From our analysis above, we find that we can eliminate the variation of the carrier density and the contact resistance with temperature as probable causes for the temperature dependence of the spin transport param-

eters. However, other mechanisms such as spin orbit coupling and the structural phase transition in STO could play a significant role in the observed variation of the spin transport parameters. The exact details of these processes are difficult to pinpoint at this stage.

Using STO as a back gate, we can tune the surface dipoles on the surface of STO at 4 K.  $\epsilon_r$  of STO increases from 300 at room temperature to more than 24,000 at 4 K (figure 5a). A modest back gate modulation of the surface dipoles through a 0.5 mm thick STO is thus realized at 4 K. Beyond 4 K, the decreased  $\epsilon_r$  leads to inefficient back gating making it difficult to draw any reasonable conclusions on the gate dependence of spin relaxation at higher temperatures. We have swept the back gate between 70 V to -40 V and wait for 600 s before the start of each spin transport measurement. As shown in figure 4e and f, the intrinsic surface dipole strength will be enhanced at negative gate voltage and reduced at positive gate voltage. As discussed before, this intrinsic electric field will affect the spin relaxation time. We observe that  $\tau_s$ ,  $D_s$  and  $\lambda_s$  increases up to a factor of two at higher positive  $V_g$ , while at negative and small positive gate voltage, these parameters do not seem to change much, as shown in figure 4.

There are two prevalent spin relaxation mechanisms in graphene. The first is the Elliot-Yafet (EY) mechanism, where the spin loses its direction by scattering with the impurities. Thus in this case, the spin-relaxation time is proportional to the momentum relaxation time. The second mechanism is the D'yakonov-Perel'(DP) mechanism, where the spin precesses in a spin-orbit field between two momentum scattering events and the spin relaxation time is inversely proportional to the momentum relaxation time. To further understand the relative contribution of the Elliot-Yafet (EY) and D'yakonov-Perel'(DP) mechanisms in our case, we assume  $D_s \approx D_c$  and calculate the momentum relaxation time  $\tau_p$  according to  $D \sim v_F^2 \tau_p$ . Following the analysis of Zomer *et al.*, Jo *et al.* and Gurram *et al.*[5, 32, 33], we analyze the relation between  $\tau_p$  and  $\tau_s$  using the equation:

$$\frac{\epsilon_F^2 \tau_p}{\tau_s} = \Delta_{EY}^2 + \left(\frac{4\Delta_{DP}^2}{\hbar^2}\right) \epsilon_F^2 \tau_p^2 \quad (2)$$

where  $\epsilon_F$  is the Fermi energy,  $\Delta_{EY}$  and  $\Delta_{DP}$  are the spin orbit coupling for EY and DP mechanism respectively. Figure 4d shows the  $\frac{\epsilon_F^2 \tau_p}{\tau_s}$  versus  $\epsilon_F^2 \tau_p^2$  dependence. From the fitting, we extract  $\Delta_{EY} = 532 \mu\text{eV}$  and  $\Delta_{DP} = 147 \mu\text{eV}$ .

We further analyze the spin relaxation mechanism in graphene on STO by considering the variation of  $\epsilon_r$  by an applied gate bias.  $\epsilon_r$  of STO can be calculated using:[34, 35]

$$\epsilon_r(T, E) = \frac{b(T)}{\sqrt{a(T) + E^2}} \quad (3)$$

where  $T$  is the temperature,  $E$  is the electric field, fitting parameters  $b(T) = 1.37 \times 10^7 + 4.29 \times 10^7 \left(\frac{T}{100}\right) \text{V/cm}$  and  $a(T) = [b(T)/\epsilon_r(T, 0)]^2 \text{V}^2/\text{cm}^2$ , and  $\epsilon_r(T, 0)$  is expressed using Barrett's formula:[36]

$$\epsilon_r(T, 0) = \frac{1635}{\text{coth}(44.1/T) - 0.937} \quad (4)$$

The calculated variation of  $\epsilon_r$  on back gate is shown in figure 5a. We incorporate the variation of  $\epsilon_r$  in our calculation of  $\epsilon_F$  using  $n = 4\epsilon_F^2 / (g_s g_v \pi \hbar^2 V_F^2) = \frac{\epsilon_r \epsilon_0}{et} \Delta V_g$ , where  $\epsilon_0$  is the vacuum permittivity and  $t$  is the thickness of STO (0.5 mm). Figure 4d is now reanalyzed considering this variation of  $\epsilon_r$  by the applied electric field and shown in figure 5b. In the new fitting (figure 5 b), we obtain  $\Delta_{EY} = 537 \mu\text{eV}$  and  $\Delta_{DP} = 162 \mu\text{eV}$  (the respective numbers in figure 4d are  $\Delta_{EY} = 532 \mu\text{eV}$  and  $\Delta_{DP} = 147 \mu\text{eV}$ ). From existing analyses of spin relaxation mechanisms in graphene on hBN and on other substrates[5, 32, 33], we find that the reported values of  $\Delta_{DP}$  vary between 40-200  $\mu\text{eV}$  and that of  $\Delta_{EY}$  between 0.5 meV and 2.3 meV. The values we have obtained from our fittings are similar to these values. Spin relaxation rates are further analyzed:  $\tau_{(s,EY)} = 0.2\text{-}5.6 \text{ ns}^{-1}$  and  $\tau_{(s,DP)} = 0.02\text{-}0.09 \text{ ns}^{-1}$ , and are of the same order for EY and DP spin relaxation. We conclude that for graphene on STO, the dominant mechanism of spin relaxation thus cannot be clearly distinguished.

We report on the first observation of spin transport in graphene on  $\text{TiO}_2$  terminated STO. A spin relaxation time and length of  $1.2 \pm 0.1 \text{ ns}$  and  $5.6 \pm 0.5 \mu\text{m}$  are obtained at 290 K, indicating that STO is a suitable substrate for studying spin transport in graphene. We find a non-trivial variation of the spin transport parameters in graphene with temperature, even in the absence of an externally applied gate voltage. Our work demonstrates that spin transport in graphene on STO is influenced by the properties intrinsic to STO, such as spin orbit coupling and structural phase transition. The strength of the surface dipoles can also be tuned by the back gate at 4 K, leading to an increase in the spin relaxation time at positive gate voltage. Our analysis of the spin relaxation time and momentum relaxation time shows that the dominant mechanism of spin relaxation cannot be established precisely. The integration of graphene with complex oxides opens new opportunities to study proximity induced functionalities at such interfaces, useful for future spintronics and optoelectronics applications.

We would like to acknowledge J. G. Holstein, H. M. de Roos, H. Adema and T. J. Schouten for their technical support and S. Omar, A. M. Kamerbeek, J. Ingla-Aynes, and A. Kaverzin for useful discussions. This work was realized using NanoLabNL (NanoNed) facilities and is a part of the 'Functional Materials' programme (project number 729.002.001), financed by the Netherlands Organisation for Scientific Research (NWO). S. Chen acknowledges funding support from the European Union Horizon 2020 research and innovation programme un-

der grant agreement No 696656 and the Spinoza Prize awarded to B. J. van Wees by NWO.

- 
- [1] C. Ertler, S. Konschuh, M. Gmitra, and J. Fabian, *Phys. Rev. B* **80**, 041405 (2009).
- [2] M. H. D. Guimarães, P. J. Zomer, J. Ingla-Aynés, J. C. Brant, N. Tombros, and B. J. van Wees, *Phys. Rev. Lett.* **113**, 086602 (2014).
- [3] W. Han, K. Pi, K. M. McCreary, Y. Li, J. J. I. Wong, A. G. Swartz, and R. K. Kawakami, *Phys. Rev. Lett.* **105**, 167202 (2010).
- [4] T. Maassen, I. J. Vera-Marun, M. H. D. Guimarães, and B. J. van Wees, *Phys. Rev. B* **86**, 235408 (2012).
- [5] P. J. Zomer, M. H. D. Guimarães, N. Tombros, and B. J. van Wees, *Phys. Rev. B* **86**, 161416 (2012).
- [6] C. R. Dean, A. F. Young, I. Meric, C. Lee, L. Wang, S. Sorgenfrei, K. Watanabe, T. Taniguchi, P. Kim, K. L. Shepard, and J. Hone, *Nat. Nanotech.* **5**, 722 (2010).
- [7] J. Ingla-Aynés, M. H. D. Guimarães, R. J. Meijerink, P. J. Zomer, and B. J. van Wees, *Phys. Rev. B* **92**, 201410 (2015).
- [8] M. Gurram, S. Omar, and B. J. van Wees, *Nat. Commun.* **8**, 248 (2017).
- [9] S. Omar and B. J. van Wees, *Phys. Rev. B* **97**, 045414 (2018).
- [10] J. A. Sulpizio, S. Ilani, P. Irvin, and J. Levy, *Annu. Rev. Mater. Res.* **44**, 117 (2014), <https://doi.org/10.1146/annurev-matsci-070813-113437>.
- [11] T. Sakudo and H. Unoki, *Phys. Rev. Lett.* **26**, 851 (1971).
- [12] A. M. Kamerbeek, P. Högl, J. Fabian, and T. Banerjee, *Phys. Rev. Lett.* **115**, 136601 (2015).
- [13] A. Sahoo, D. Nafday, T. Paul, R. Ruiter, A. Roy, M. Mostovoy, T. Banerjee, T. Saha-Dasgupta, and A. Ghosh, *npj 2D Materials and Applications* **2**, 9 (2018).
- [14] F. W. Lytle, *J. Appl. Phys.* **35**, 2212 (1964).
- [15] M. Honig, J. A. Sulpizio, J. Drori, A. Joshua, E. Zeldov, and S. Ilani, *Nat. Mater.* **12**, 1112 (2013).
- [16] Y. Frenkel, N. Haham, Y. Shperber, C. Bell, Y. Xie, Z. Chen, Y. Hikita, H. Y. Hwang, E. K. H. Salje, and B. Kalisky, *Nat. Mater.* **16**, 1203 (2017).
- [17] N. Couto, B. Sacépé, and A. Morpurgo, *Phys. Rev. Lett.* **107**, 225501 (2011).
- [18] N. J. Couto, D. Costanzo, S. Engels, D.-K. Ki, K. Watanabe, T. Taniguchi, C. Stampfer, F. Guinea, and A. F. Morpurgo, *Phys. Rev. X* **4**, 041019 (2014).
- [19] R. Sachs, Z. Lin, and J. Shi, *Sci. Rep.* **4**, 3657 (2014).
- [20] S. Saha, O. Kahya, M. Jaiswal, A. Srivastava, A. Annadi, J. Balakrishnan, A. Pachoud, C.-T. Toh, B.-H. Hong, J.-H. Ahn, T. Venkatesan, and B. Özyilmaz, *Sci. Rep.* **4**, 6173 (2014).
- [21] K. T. Kang, H. Kang, J. Park, D. Suh, and W. S. Choi, *Adv. Mater.* **29**, 1700071 (2017), arXiv:1705.05672.
- [22] H. Ryu, J. Hwang, D. Wang, A. S. Disa, J. Denlinger, Y. Zhang, S.-K. Mo, C. Hwang, and A. Lanzara, *Nano Lett.* **17**, 5914 (2017).
- [23] S. Adam, E. H. Hwang, V. M. Galitski, and S. D. Sarma, *Proc. Natl. Acad. Sci.* **104**, 18392 (2007).
- [24] M. Kawasaki, K. Takahashi, T. Maeda, R. Tsuchiya, M. Shinohara, O. Ishiyama, T. Yonezawa, M. Yoshimoto, and H. Koinuma, *Science* **266**, 1540 (1994).
- [25] G. Koster, B. L. Kropman, G. J. H. M. Rijnders, D. H. A. Blank, and H. Rogalla, *Appl. Phys. Lett.* **73**, 2920 (1998).
- [26] P. J. Zomer, M. H. D. Guimarães, J. C. Brant, N. Tombros, and B. J. v. Wees, *Appl. Phys. Lett.* **105**, 013101 (2014).
- [27] M. Popinciuc, C. Józsa, P. J. Zomer, N. Tombros, A. Veligura, H. T. Jonkman, and B. J. van Wees, *Phys. Rev. B* **80**, 214427 (2009).
- [28] J. Fabian, A. Matos-Abiague, C. Ertler, P. Stano, and I. Žutić, *Acta Phys. Slovaca* **57**, 565 (2007).
- [29] E. Heifets, E. A. Kotomin, and J. Maier, *Surf. Sci.* **462**, 19 (2000).
- [30] B. Meyer and D. Vanderbilt, *Phys. Rev. B* **63**, 205426 (2001).
- [31] D. Kochan, M. Gmitra, and J. Fabian, *Phys. Rev. Lett.* **112**, 116602 (2014).
- [32] S. Jo, D.-K. Ki, D. Jeong, H.-J. Lee, and S. Kettemann, *Phys. Rev. B* **84**, 075453 (2011).
- [33] M. Gurram, S. Omar, S. Zihlmann, P. Makk, Q. C. Li, Y. F. Zhang, C. Schönenberger, and B. J. Van Wees, *Phys. Rev. B* **97**, 045411 (2018), arXiv:1712.00815.
- [34] A. M. Kamerbeek, T. Banerjee, and R. J. E. Huetting, *J. Appl. Phys.* **118**, 225704 (2015).
- [35] S. Suzuki, T. Yamamoto, H. Suzuki, K. Kawaguchi, K. Takahashi, and Y. Yoshisato, *J. Appl. Phys.* **81**, 6830 (1997).
- [36] J. H. Barrett, *Phys. Rev.* **86**, 118 (1952).

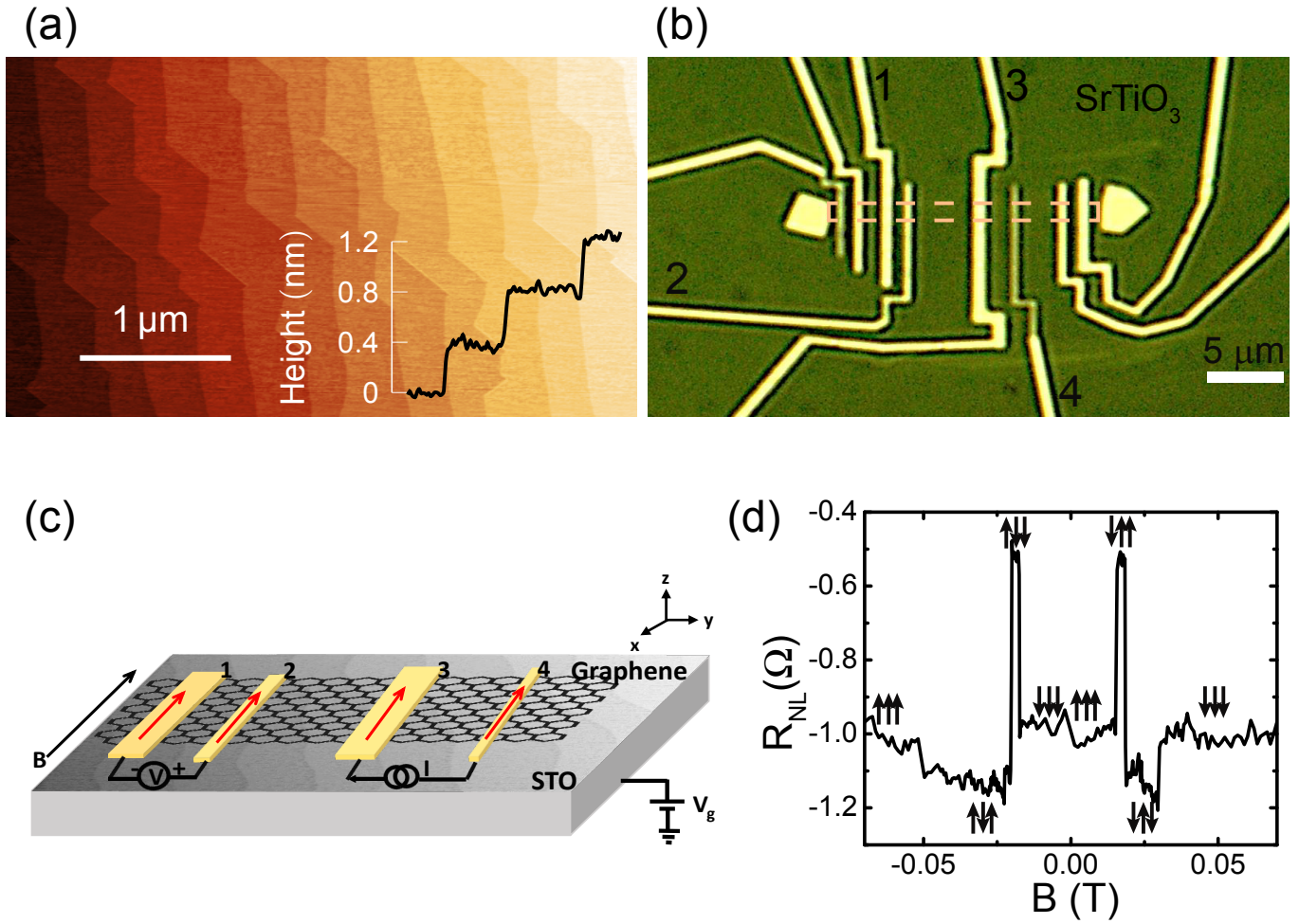


FIG. 1. (a) Atomic force microscope image of a  $\text{TiO}_2$  terminated STO substrate after surface treatment and annealing at  $960^\circ\text{C}$ . The inset shows a height profile of the terrace steps. (b) Optical microscope image of the device.  $\text{Co}/\text{AlO}_x$  contacts are in yellow and the graphene flake is indicated by the orange dash line. (c) Schematic of the measurement circuit, where the  $\text{Co}/\text{AlO}_x$  electrodes are in gold. A current is injected through contact 3 and detected by contact 1-2. (d) Measurement of a non-local spin valve at 290 K. Three switches are seen, which corresponds to the contact 1, 3, 2.

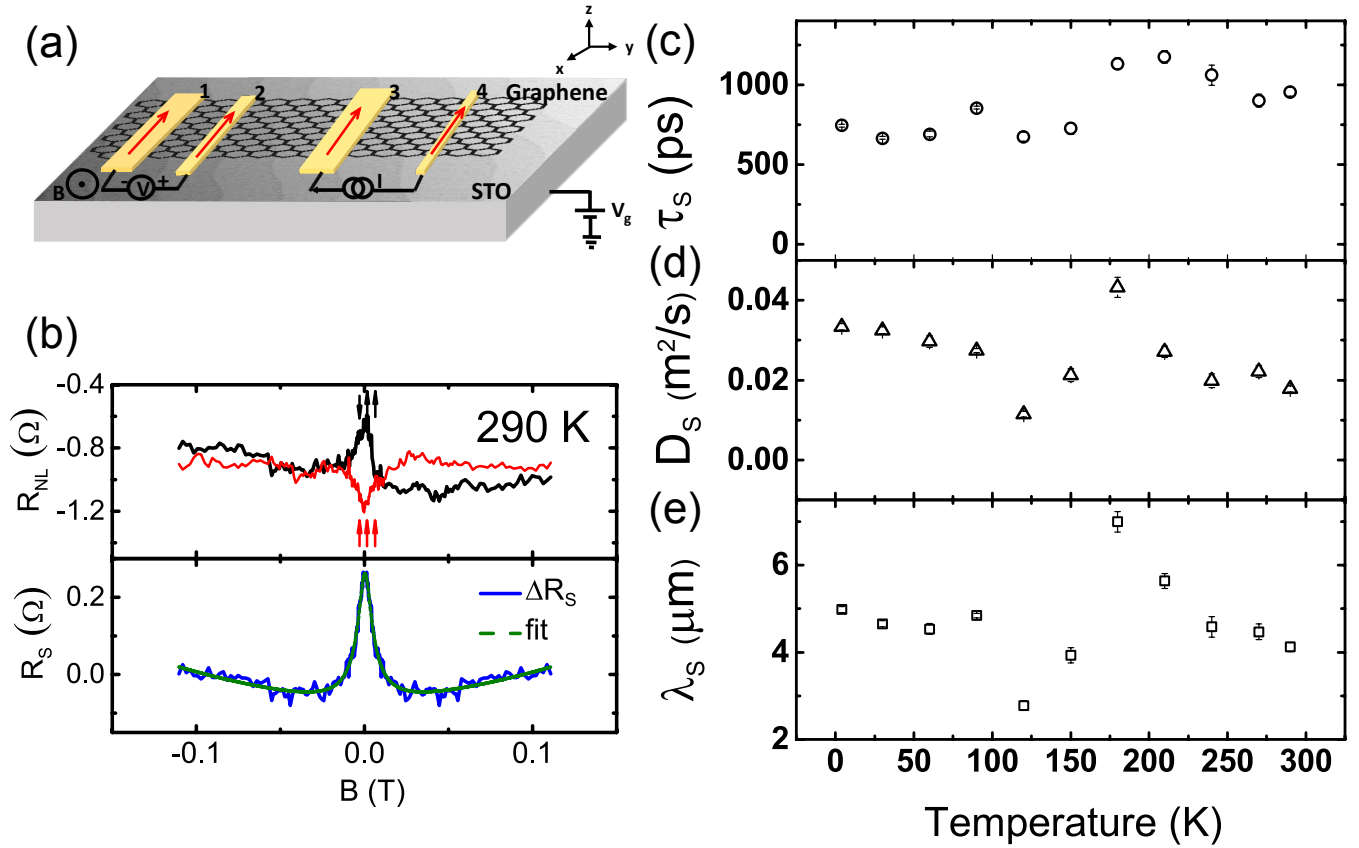


FIG. 2. (a) Schematic of Hanle measurements with magnetic field out of plane. (b) Hanle measurements of  $\downarrow\uparrow$  (black) and  $\uparrow\uparrow$  (red) configurations of contact 1, 2, 3 respectively and calculated Hanle signal (blue) after the background subtraction fitted with the steady state solution to the Bloch equation in the diffusive regime. (c) The extracted spin relaxation time  $\tau_s$ , (d) spin diffusion constant  $D_s$  and (e) the calculated spin relaxation length  $\lambda_s = \sqrt{D_s \tau_s}$  as a function of temperature from Hanle measurements. Error bars are derived from fitting errors.

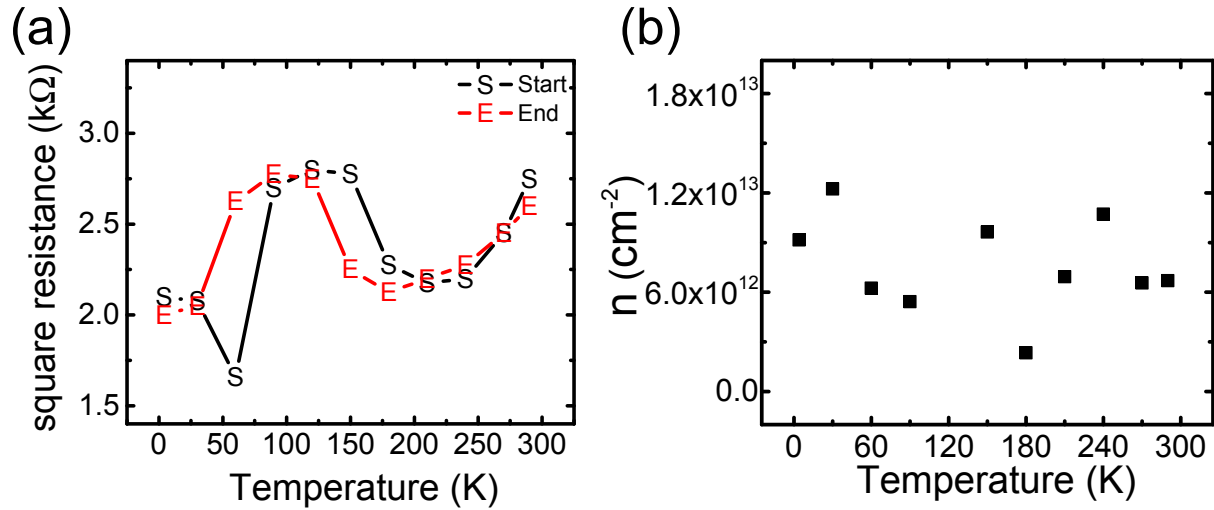


FIG. 3. (a) Square resistance of the graphene channel used for the Hanle measurements shown in figure 2b. The square resistance was measured at the start and at the end of a measurement sequence for each measurement temperature. (b) Carrier density versus temperature calculated from spin diffusion constant  $D_s$  and square resistance  $R_{sq}$  of graphene

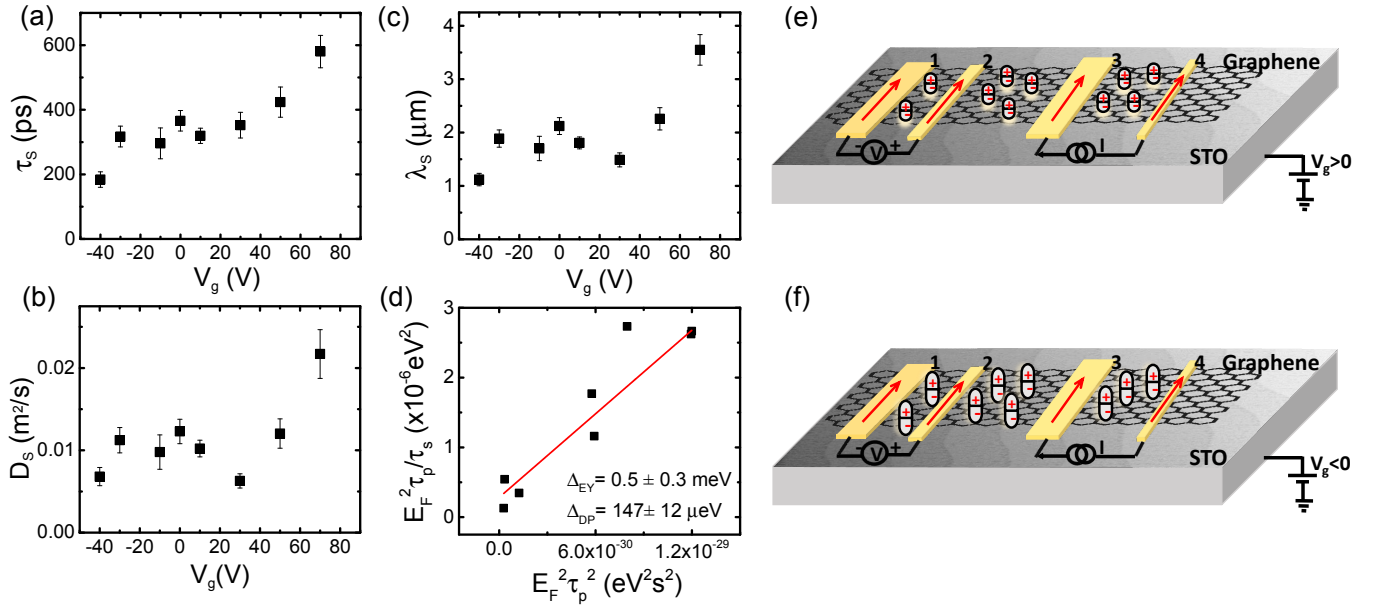


FIG. 4. Gate dependent spin transport parameters at 4 K. (a) (b) (c) gate dependence of  $\tau_s$ ,  $D_s$  and  $\lambda_s$ . The gate is swept between 70 V to  $-70$  V. Higher  $\tau_s$ ,  $D_s$  and  $\lambda_s$  values are observed at positive positive gate voltage. Note: below  $-40$  V, the Hanle curves cannot be fitted with the steady state solution to the one-dimensional Bloch equation. (d)  $\frac{\epsilon_F^2 \tau_p}{\tau_s}$  versus  $\epsilon_F^2 \tau_p^2$  at 4 K. The solid line is the fit using Equation 2. The error bars are the fitting errors. (e)(f) Surface dipoles at  $V_g > 0$  and  $V_g < 0$ . At positive gate voltage, the surface dipoles are suppressed by the electric field; at negative gate voltage, the surface dipoles are enhanced.

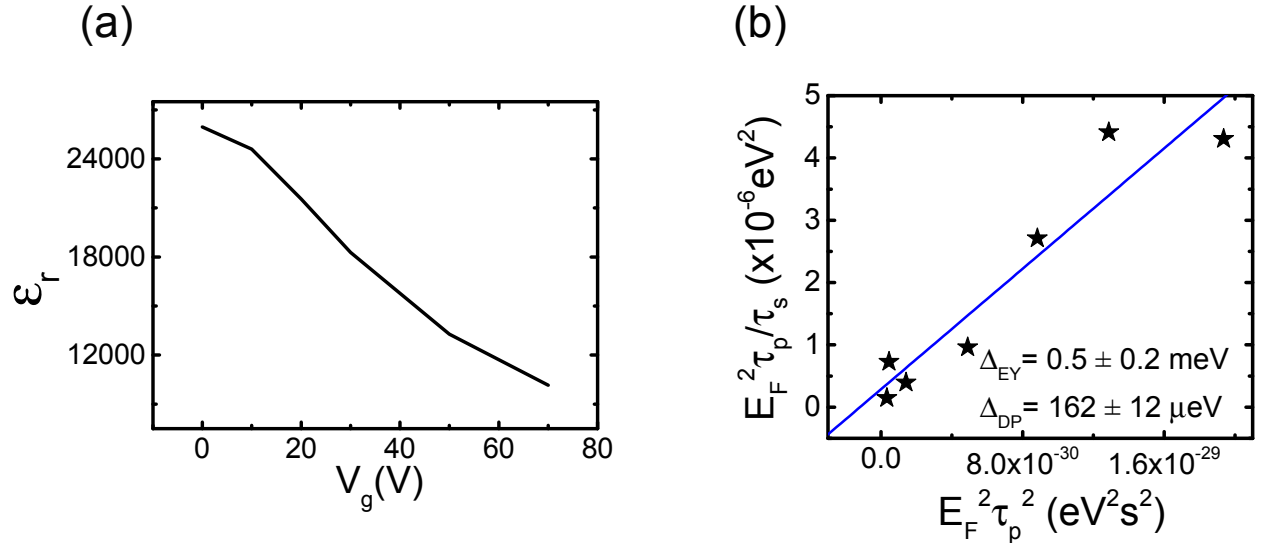


FIG. 5. (a) Gate dependent  $\epsilon_r$  at 4 K calculated using Eq.3. (b)  $\frac{\epsilon_F^2 \tau_p}{\tau_s}$  versus  $\epsilon_F^2 \tau_p^2$  at 4 K taking into account the variation of  $\epsilon_r$  with gate bias. The calculated data points incorporating the dielectric constant correction is represented by the stars and the blue solid line is the fit using Equation 2. The error bars are the fitting errors.